a site exchange between transition-metal and main-group elements has been observed for several structure types (see *e.g.* Parthé & Chabot, 1984). As mentioned above, a site exchange is also observed for ternary silicide and aluminide substitution derivatives of Th_6Mn_{23}, the transition-metal element (Ni) in $Hf_6Ni_7Al_{16}$ occupying the same sites as the main-group element (Si) in $Mg_6Cu_{16}Si_7$. Ternary Ru-based aluminides of approximate composition $R_6Ru_7Al_{16}$ (R = Sc, Ti or Zr), have also been reported with this structure type (Markiv & Storozhenko, 1973).

We wish to acknowledge the help of Ms Birgitta Künzler with the drawings. This study was supported by the Swiss National Science Foundation under contract 20-28490.90.

References

ANDRUSYAK, R. I. (1988). *Sov. Phys. Crystallogr.* **33**, 599–600.
BERGMAN, G. & WAUGH, J. L. T. (1956). *Acta Cryst.* **9**, 214–217.
BLANC, E., SCHWARZENBACH, D. & FLACK, H. D. (1991). *J. Appl. Cryst.* **24**, 1035–1041.
DEBAERDEMAEKER, T., GERMAIN, G., MAIN, P., TATE, C. & WOOLFSON, M. M. (1987). *MULTAN87. A System of Computer Programs for the Automatic Solution of Crystal Structures from X-ray Diffraction Data.* Univs. of York, England, and Louvain, Belgium.
EDSHAMMAR, L. E. (1965). *Acta Chem. Scand.* **19**, 2124–2130.
ERASSME, J. & LUEKEN, H. (1987). *Acta Cryst.* B**43**, 244–250.
FLORIO, J. V., RUNDLE, R. E. & SNOW, A. I. (1952). *Acta Cryst.* **5**, 449–457.
FORNASINI, M. L. (1971). *J. Less-Common Met.* **25**, 329–332.
GANGLBERGER, E., NOWOTNY, H. & BENESOVSKY, F. (1966). *Monatsh. Chem.* **97**, 829–832.
GELATO, L. M. & PARTHÉ, E. (1987). *J. Appl. Cryst.* **20**, 139–143.
GLADYSHEVSKII, R. E., CENZUAL, K., FLACK, H. D. & PARTHÉ, E. (1993). *Acta Cryst.* B**49**, 468–474.
GLADYSHEVSKII, R. E., CENZUAL, K. & PARTHÉ, E. (1992). *J. Alloys Comp.* **182**, 165–170.
GLADYSHEVSKII, R. E. & PARTHÉ, E. (1992). *Z. Kristallogr.* **198**, 171–172.
HALL, S. R. & STEWART, J. M. (1990). Editors. *XTAL3.0 Users Manual.* Univs. of Western Australia, Australia, and Maryland, USA.
KOTUR, B. YA., SIKIRITSA, M., BODAK, O. I. & GLADYSHEVSKII, E. I. (1983). *Sov. Phys. Crystallogr.* **28**, 387–389.
MARKIV, V. YA. & STOROZHENKO, A. I. (1973). *Dopov. Akad. Nauk Ukr. RSR Ser. A*, **10**, 941–943.
MERLO, F. & FORNASINI, M. L. (1982). *Acta Cryst.* B**38**, 1797–1798.
MÜHLPFORDT, W. (1970). *Z. Anorg. Allg. Chem.* **374**, 174–185.
PARTHÉ, E. & CHABOT, B. (1984). *Handbook on the Physics and Chemistry of the Rare Earths*, edited by K. A. GSCHNEIDNER JR & L. EYRING, Vol. 6, ch. 48, pp. 113–334. Amsterdam: North Holland.
RYKHAL', R. M., ZARECHNYUK, O. S. & MARYCH, O. M. (1978). *Dopov. Akad. Nauk Ukr. RSR Ser. A*, **9**, 853–855.
WANG, F. E., KANDA, F. A., MISKELL, C. F. & KING, A. J. (1965). *Acta Cryst.* **18**, 24–31.

Acta Cryst. (1993). B**49**, 478–483

Structure of a High-Pressure Polymorph of Mg_3BN_3 Determined from X-ray Powder Data

BY HIDEO HIRAGUCHI,* HIROO HASHIZUME† AND SATOSHI SASAKI

Research Laboratory of Engineering Materials, Tokyo Institute of Technology, Nagatsuta, Midori, Yokohama 227, *Japan*

AND SATOSHI NAKANO AND OSAMU FUKUNAGA

Department of Inorganic Materials, Faculty of Engineering, Tokyo Institute of Technology, Ookayama, Meguro, Tokyo 152, *Japan*

(*Received* 31 *July* 1992; *accepted* 23 *December* 1992)

Abstract

The crystal structure of magnesium boron nitride in a high-pressure phase, $Mg_3NB_3(H)$, has been determined from X-ray powder diffraction data. The strategy used was: powder pattern indexing, extraction of integrated intensity data by peak decomposition, Patterson function calculation, trial-and-error model building and Rietveld refinement. The cell is orthorhombic (space group *Pmmm*, $Z = 1$) with $a = 3.0933\ (2)$, $b = 3.1336\ (2)$ and $c = 7.7005\ (5)$ Å. The structure contains linear NBN groups with an observed B—N interatomic distance of 1.34 Å which is 2% shorter than in the low-pressure form of the material, $Mg_3BN_3(L)$. The double-bonded N=B=N molecular anions are believed to play an important role in the recently reported decomposition of

* Present address: The Tokyo Electric Power Co. Inc., 1-1-3 Uchisaiwaicho, Chiyoda, Tokyo 100, Japan.
† To whom all correspondence should be addressed.

0108-7681/93/030478-06$06.00

$Mg_3BN_3(H)$ in the synthesis of cubic boron nitride under high-pressure/high-temperature conditions. The JCPDS file No. for Mg_3BN_3 is 44-1497.

Introduction

Magnesium boron nitride, Mg_3BN_3, is a useful catalyst in the conversion of hexagonal boron nitride, *h*BN, to the cubic form (*c*BN) under high-pressure/high-temperature conditions (Wentrof, 1961; Endo, Fukunaga & Iwata, 1979; Sato, 1986). Mg_3BN_3 crystallizes in a number of different forms depending on the pressure and temperature applied. The low-pressure polymorph $Mg_3BN_3(L)$ has a hexagonal cell with $a = 3.54453\ (4)$ and $c = 16.0353\ (3)$ Å (space group $P6_3/mmc$, $Z = 2$) (Hiraguchi, Hashizume, Fukunaga, Takenaka & Sakata, 1991). The structure contains linear N=B=N molecular anions parallel to the *c* axis, which are believed to play a role in the catalytic property of the material. A high-pressure form was first reported by Endo *et al.* (1979) who published a $d - I$ table, obtained from X-ray Debye–Scherrer patterns of a yellowish compound synthesized from a mixture of Mg metal and *h*BN powder at 2.5 GPa and 1423 K. The stoichiometry of the compound was reported to be $Mg_3B_2N_4$ on the basis of chemical analysis. The results were challenged by Elyutin *et al.* (1981) who claimed that Endo's compound was not a phase but a mixture of the so-called α- and β-phases of $Mg_3B_2N_4$. Hohlfeld (1989) proposed another phase relation, where Mg_3BN_3 was an intermediate product during the formation of $Mg_3B_2N_4$ from a *h*BN–Mg_3N_2 system and the two compounds coexisted at 6.5 GPa and 1600–1650 K. A phase transition of $Mg_3BN_3(L)$ to a high-pressure polymorph, $Mg_3BN_3(H)$, was evidenced by Nakano, Ikawa & Fukunaga (1992), who located the phase boundary at 773 K, 5.5 GPa and 1173 K, 4.0 GPa. No structure determination has been reported for the high-pressure phases of the Mg–B–N system, however.

There is increasing interest in structure determination from powder diffraction data (McCusker, 1992). Small structures can be solved *ab initio* using an orthodox method which decomposes a powder pattern into individual Bragg peaks to extract integrated intensity data and uses standard single-crystal structure-solving techniques involving Patterson and direct methods. Once an approximate structure is obtained, Rietveld programs can be run to refine the structure. Quite a few structures have been solved using this approach (McCusker, 1988; Hiraguchi *et al.*, 1991, and references therein). Large structures are more difficult to solve because of peak overlaps, caused by finite instrumental resolution and crystal symmetry, which limit the data resolution. Various approaches have recently been proposed to estimate the overlapping intensities as accurately as possible (Jansen, Pescher & Schenk, 1992; Cascarano, Favia & Giacovazzo, 1992; Estermann & Gramlich, 1992), but routine methods have yet to be established. The maximum-entropy technique provides another way of handling the problem (Gilmore, Henderson & Bricogne, 1991).

In the present paper we will adopt the orthodox approach in order to determine the structure of $Mg_3BN_3(H)$ from X-ray powder data.

Sample preparation and data collection

Low-pressure $Mg_3BN_3(L)$ was synthesized by a procedure outlined by Nakano *et al.* (1992), which is not quite the same as the one described in our previous publication (Hiraguchi *et al.*, 1991). The present procedure uses a starting material of mixed *h*BN powder and Mg metal flakes in approximately 1:3 molar ratio with a slight excess of *h*BN. The first step is to place the material in an uncapped steel capsule (inner diameter 1 cm, depth 5 cm) in an oven filled with flowing N_2 gas. The oven is heated to 873 K over 2 h, held constant at this temperature for 4 h and then cooled. Next, a screw cap is placed on the capsule and the oven temperature raised to 1473 K over 4 h, then held constant at this temperature for 10 h with N_2 gas flowing through the oven. Mg is nitrogenized in the first step to produce Mg_3N_2 by the reaction $3Mg + N_2 \rightarrow Mg_3N_2$, while the second step promotes the reaction $Mg_3N_2 + hBN \rightarrow Mg_3BN_3(L)$. We pulverized the cooled yellow product and stored it in a glass bottle.

$Mg_3BN_3(L)$, prepared thus, was transformed to $Mg_3BN_3(H)$ in a high-pressure apparatus using cubic anvils (Nakano *et al.*, 1992). We compressed $Mg_3BN_3(L)$ powder in a nitrogen atmosphere, to form a thin disk which was then wrapped in platinum foil to avoid contact with the inner wall of a cylindrical open-ended NaCl cell. The charged cell was placed inside a tubular carbon heater (inner diameter 5 mm) with NaCl disks sandwiching the wrapped $Mg_3BN_3(L)$ disk from each side. The assembly, with associated electrodes, was placed in a 6 mm hole drilled in a 13 mm cube of baked pyrophyllite, which was mounted on the cubic anvil press. Under compression, this material fills the gap and acts as a pressure medium, like the NaCl. The conversion $Mg_3BN_3(L) \rightarrow Mg_3BN_3(H)$ took place at 4.0 GPa and 1573 K in 15 min. The product was pulverized and examined on an X-ray diffractometer. We repeated seven high-pressure runs in order to collect a 0.3 cm^3 volume of powder, which was stored in an evacuated box prior to the X-ray experiments – Mg_3BN_3 crystals absorb water vapour from the air and become denatured.

X-ray data were collected under ambient conditions on a JEOL θ–θ powder diffractometer using standard slits and a pyrolytic graphite diffracted-beam analyzer located at a copper tube source. Two scans were performed over a 10–140° 2θ range in steps of 0.02°. The first scan with a count time of 5 s per step was accidentally interrupted at $2\theta = 68°$ and no further data were available. The second scan, with a 20 s count time per step, successfully explored the intended 2θ range. Sharp reflections were observed together with a few low peaks from MgO, $Mg(OH)_2$, *h*BN and *c*BN, present in the sample as impurities.

Structure determination

We selected 11 strong reflections from the first data set and determined their peak positions using the peak-fitting program *PRO-FIT* (Toraya, 1986). The information obtained was input to the program *DICVOL*91 (Boultif & Louër, 1991), which indexed the given reflections on an orthorhombic cell with $a = 3.0931$ (8), $b = 3.1344$ (8), $c = 7.6977$ (21) Å and $V = 74.630$ Å^3. The figures of merit obtained, $M_{11} = 71.5$ and $F_{11} = 27.7$, indicate a good indexing result. No systematic extinction was observed, which suggests *P*222, *Pmm*2 and *Pmmm* as possible space groups. Integrated intensities of individual lines are usually determined using the whole-pattern fitting technique. Such attempts, however, yielded no satisfactory profile fit in the present case because of the irregular peak shapes observed. We then ran *PRO-FIT* to individually fit peaks in the $10 < 2\theta < 73°$ range. Fig. 1 shows four Mg_3BN_3(*H*) peaks decomposed by *PRO-FIT*. Clearly, the high-angle peak shows a narrower width than the low-angle peak. Peak widths plotted against 2θ are scattered, yet different 2θ dependences are observed depending on the *hkl* type (Fig. 2). This explains why a whole-pattern fitting with a single set of peak-width parameters for all reflections did not work. The abnormal peak behavior could have its origin in specific crystallite shapes or defect structures, but no further investigation was attempted. Of the 34 symmetry-allowed reflections, 13 were allocated no statistically significant intensity in the pattern decomposition. These intensities were set to zero. The effective resolution of the intensity data was 1.305 Å.

After multiplicity and Lp corrections, the integrated intensities were used to calculate Patterson functions. The intensity statistics did not allow judgements to be made concerning the existence of centrosymmetry and so we assumed *Pmmm* for Mg_3BN_3(*H*), which has the highest symmetry among the possible space groups. It was observed that Patterson maxima only lie in the (110) plane. Major peaks were taken to represent the Mg–*X* correlations, where *X* is one of the atoms Mg, B and N. Fig. 3 shows the (110) Patterson map compared with the $(11,\bar{2},0)$ map for the previously solved Mg_3BN_3(*L*) (Hiraguchi *et al.*, 1991). The common features in the two maps suggest a similar atomic configuration in the required structure. With $Z = 1$ in mind, inferred from the observed unit-cell volume, we built trial-and-error model structures of Mg_3BN_3(*H*), compatible with the symmetry and interatomic vector information, from which simulated powder patterns were generated and compared with observation. The most likely model had Mg atoms at 1(*a*) (0, 0, 0) and 2(*t*) ($\frac{1}{2}$, $\frac{1}{2}$, z_1) with $z_1 \simeq \frac{1}{4}$, B atoms at 1(*c*) (0, 0, $\frac{1}{2}$), N atoms at 1(*f*) ($\frac{1}{2}$, $\frac{1}{2}$, 0) and 2(*q*) (0, 0, z_2) with $z_2 \simeq \frac{1}{3}$. Rietveld refinements of this structure used the program *PFLS* (Toraya & Marumo, 1980), and assumed a three-phase system of Mg_3BN_3(*H*), MgO and *c*BN. Only the cell parameters were refined for the latter compounds. It was not of interest to us to determine the abundances of these compounds from the scale factors. Data were

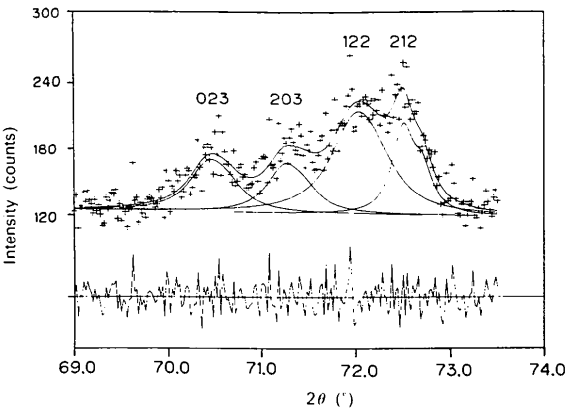

Fig. 1. Decomposition of overlapping Mg_3BN_3(*H*) peaks by *PRO-FIT*. The bottom trace shows a difference profile. Note the narrower widths of the high-angle peaks.

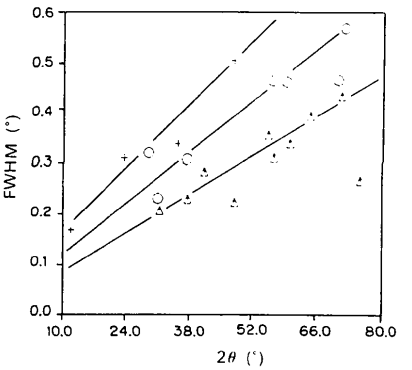

Fig. 2. Powder line widths (FWHM) of Mg_3BN_3(*H*) plotted against 2θ: +, 00*l*; ○, *hkl* ($h < k$); △, *hkl* ($h \geq k$) reflections. Lines are aids to the eyes.

discarded in the regions of *h*BN, $Mg(OH)_2$ and unidentified ($2\theta = 38.38$, 39.74, 42.78°) peaks where no $Mg_3BN_3(H)$ peak was observed. The $Mg_3BN_3(H)$ reflections were classified into three groups according to *hkl* type (see Fig. 2). For each group independent peak-width parameters (w_1, w_2, w_3) were refined, where peak width W is given by $W = (w_1 + w_2\tan\theta + w_3\tan^2\theta)^{1/2}$. The least-squares profile fit converged to $R_{wp} = 13.35\%$ ($R_e = 7.79\%$) with $z_1 = 0.2706$ (3), $z_2 = 0.3252$ (6) and an overall isotropic temperature factor coefficient $B = 2.292$ Å^2 for $Mg_3BN_3(H)$. The $Mg_3BN_3(H)$ cell parameters refined to $a = 3.0933$ (2), $b = 3.1336$ (2), $c = 7.7005$ (5) Å. Further refinements were carried out with variable parameters for Mg site occupancies (g) and for individual temperature-factor coefficients (B_i). The Mg and N positions (z_1, z_2) were also refined. The refinements resulted in a slightly better profile fit with $R_{wp} = 12.62\%$, $R_p = 9.98\%$ ($R_e = 7.80\%$). The crystallographic details are summarized in Table 1 and the final refined $Mg_3BN_3(H)$ structural parameters in Table 2. Fig. 4 plots the observed, calculated and difference profiles.*

Attempts to solve the structure assuming the non-centrosymmetric space groups *P*222 and *Pmm*2 were unsuccessful. We failed to work out a structure model consistent with the chemical and symmetry information, yet reproducing the observed powder pattern.

* Data for the observed profiles for high-pressure Mg_3BN_3 have been deposited with the British Library Document Supply Centre as Supplementary Publication No. SUP 55885 (13 pp.). Copies may be obtained through The Technical Editor, International Union of Crystallography, 5 Abbey Square, Chester CH1 2HU, England. [CIF reference: OH0030]

Table 1. *Crystallographic data for high-pressure* Mg_3BN_3 *at* 298 K

Space group	*Pmmm*
a (Å)	3.0933 (2)
b (Å)	3.1336 (2)
c (Å)	7.7005 (5)
Z	1
Wavelength (Å)	1.540562 ($K\alpha_1$) 1.544390 ($K\alpha_2$)
Pattern 2θ range (°)	10 140
Step size (°)	0.02
Number of observation points (N)	6501
Number of contributing reflections	107
Number of structural parameters ($P1$)	9
Number of profile parameters ($P2$)	8
$R_I = \sum\|I(\text{obs}) - I(\text{cal})\|/\sum I(\text{obs})$	0.1724
$R_F = \sum\|(\text{obs})^{1/2} - I(\text{cal})^{1/2}\|/\sum I(\text{obs})^{1/2}$	0.1462
$R_P = \sum\|y_i(\text{obs}) - y_i(\text{cal})\|/\sum y_i(\text{obs})$	0.0998
$R_{wp} = \{\sum w_i[y_i(\text{obs}) - y_i(\text{cal})]^2/\sum w_i y_i(\text{obs})^2\}^{1/2}$	0.1262
$R_e = [(N - P1 - P2)/\sum w_i y_i(\text{obs})^2]^{1/2}$	0.0780

Table 2. *Rietveld-refined positional, thermal and occupancy* (g) *parameters for high-pressure* Mg_3BN_3

Numbers in parentheses are the e.s.d.'s in units of the least-significant digit given. Those parameters without e.s.d.'s were held fixed in least-squares refinement.

		x	y	z	B_i (Å^2)	g
Mg(1)	1(*a*)	0	0	0	2.6 (1)	0.847 (4)
Mg(2)	2(*i*)	$\frac{1}{2}$	$\frac{1}{2}$	0.2670 (3)	1.97 (8)	0.930 (5)
N(1)	1(*f*)	$\frac{1}{2}$	$\frac{1}{2}$	0	0.9 (2)	1.0
N(2)	2(*q*)	0	0	0.3262 (5)	3.9 (1)	1.0
B	1(*c*)	0	0	$\frac{1}{2}$	4.9 (4)	1.0

Discussion

The $Mg_3BN_3(H)$ structure obtained explains well the major lines in the $d - I$ tables for $Mg_3B_2N_4$ given by Endo *et al.* (1979) and Hohlfeld (1989), but not those reported by Hohlfeld (1989) for high-pressure Mg_3BN_3. Clearly the material expressed as $Mg_3B_2N_4$

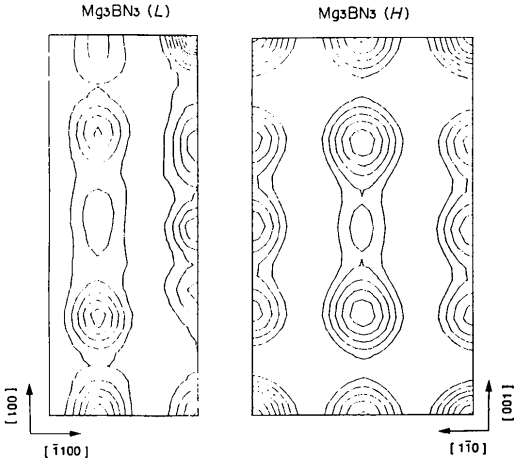

Fig. 3. Sectioned Patterson maps for the (11,$\bar{2}$,0) and (110) planes of the low- (left) and high-pressure (right) polymorphs of Mg_3BN_3. A quadrant of a unit cell is shown for the former map. The c axis is parallel to the vertical direction.

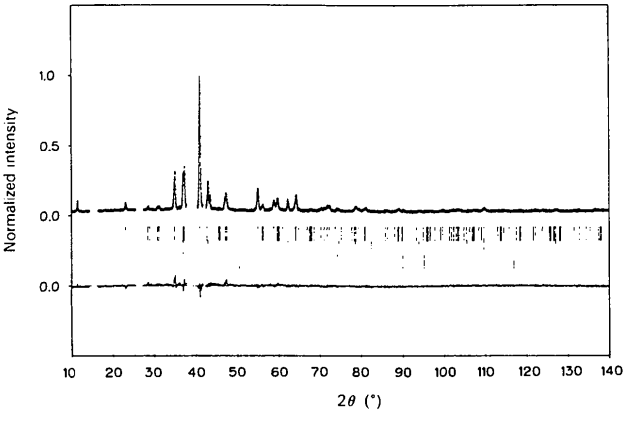

Fig. 4. Observed (crosses), calculated (full line) and difference (bottom trace) X-ray diffraction profiles for high-pressure Mg_3BN_3 powder. The difference trace plots $y_i(\text{obs}) - y_i(\text{cal})$ where $y_i(\text{obs})$ and $y_i(\text{cal})$ are observed and calculated intensities at step i. Short vertical bars mark the Bragg peak positions. Top row: $Mg_3BN_3(H)$, center row: MgO, bottom row: *c*BN. The maximum observed X-ray count is 3423.

by these authors includes $Mg_3BN_3(H)$ as the principal component. Agreement is even better with Elyutin's table for α-$Mg_3B_2N_4$ (Elyutin *et al.*, 1981) with only one incompatible entry at $d = 1.814$ Å, as pointed out by Nakano *et al.* (1992). Actually, the latter authors identified the $Mg_3BN_3(H)$ phase in their X-ray patterns largely due to the early results of the present work. The $Mg_3BN_3(H)$ cell is quasitetragonal ($b/a = 1.013$), but the unequal a and b lengths are evidenced beyond doubt by the split hkl and khl reflections (see Fig. 1).

The determined structure of $Mg_3BN_3(H)$ is compared with that of $Mg_3BN_3(L)$ in Fig. 5. The figure reveals an evident correlation of the two structures, which leads us to speculate that at high pressure/high temperature the Mg(2) and N(1) atoms in the $Mg_3BN_3(L)$ structure shift to the more symmetrical central positions, with a concomitant change of the hexagonal cell into an othorhombic cell, to produce the $Mg_3BN_3(H)$ structure. The symmetry of the resultant structure will halve the c axis, which was found to be contracted by 4% in the present study. This picture does not explain the unequal a and b lengths of the orthorhombic $Mg_3BN_3(H)$ cell, the origin of which is unclear at present. It is interesting, however, to note that the observed b/a ratio is close to 1.044, reported for a high-pressure phase of iodine at 30 GPa with a body-centered orthorhombic cell (Takemura, Minomura, Shimomura & Fujii, 1980). The a and b edges of $Mg_3BN_3(H)$ are shorter by

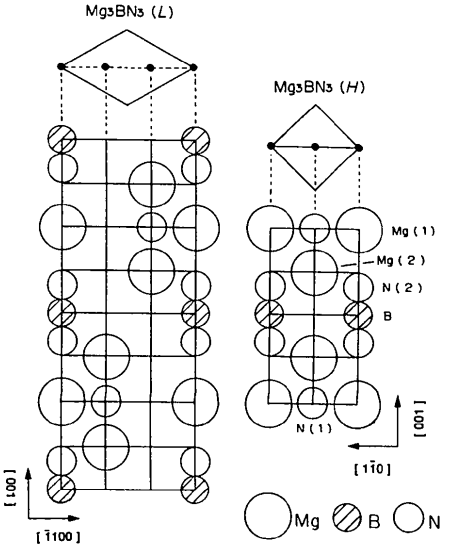

Fig. 5. Crystal structures of low- (left) and high-pressure (right) Mg_3BN_3. A $(11,\bar{2},0)$ cross section for $Mg_3BN_3(L)$ and a (110) cross section for $Mg_3BN_3(H)$. The c axis is parallel to the vertical direction. Mg: large open circles, B: small hatched circles, N: medium open circles.

Table 3. *Interatomic distances in low- and high-pressure polymorphs of* Mg_3BN_3 (Å)

	$Mg_3BN_3(L)$	$Mg_3BN_3(H)$
Mg(1)—N(1)	2.046 (0)	2.202 (0)
—N(2)	2.644 (3)	2.512 (4)
Mg(2)—N(1)	2.040 (0)	2.056 (2)
—N(2)	2.134 (1)	2.248 (1)
B—N(2)	1.365 (3)	1.338 (4)

12.7–11.6% than the a edge of the original $Mg_3BN_3(L)$ hexagonal cell.

The contracted c edge is associated with the reduced Mg(1)—N(2) and B—N(2) interatomic distances, but the Mg(1)—N(1) and Mg(2)—N(2) distances are longer in $Mg_3BN_3(H)$ than in $Mg_3BN_3(L)$ (Table 3). The B—N(2) distance undergoes the least change (−2.0%) through the $L \rightarrow H$ phase transition, indicating high mechanical rigidity of the N=B=N double bond (Hiraguchi *et al.*, 1991). The observed B—N bond length (1.338 Å) in the linear NBN group is very close to that found in bis(benzyl-*tert*-butylamino)boron tetrachloroaluminate, Li_3BN_2 and Na_3BN_2 [see Hiraguchi *et al.* (1991) for references]. These compounds were reported to include quasilinear NBN bonds. It is also close to the Hartree–Fock calculation result (1.373 Å) obtained by Pyykkö & Zhao (1990).

The quality of our data does not justify quantitative discussion of the site occupancies (g) and the thermal vibration of individual atoms. Good qualitative agreement is found, however, between the B_i parameters of $Mg_3BN_3(L)$ (Hiraguchi *et al.*, 1991) and those given in Table 1. In both structures the B and N(2) atoms vibrate the most vigorously and the N(1) atoms are the quietest. It would be more than a coincidence that the g values for the Mg(1) and Mg(2) atoms in Table 1 are very close to their counterparts in $Mg_3BN_3(L)$ (Hiraguchi *et al.*, 1991). Appreciable fractions of the Mg atoms are likely to be missing from the Mg sites in both $Mg_3BN_3(L)$ and $Mg_3BN_3(H)$ crystals.

Nakano *et al.* (1992) postulated 'isolated' NBN groups to explain the synthesis of cBN by decomposition of water-containing $Mg_3BN_3(H)$ at pressures higher than 4 GPa. The double bond, N=B=N, in low-pressure $Mg_3BN_3(L)$ was confirmed by the infrared absorption data (Hiraguchi *et al.*, 1991). The very similar atomic configuration of NBN in high-pressure $Mg_3BN_3(H)$ illustrates a remarkable stability of this double bond through the phase transformation $Mg_3BN_3(L) \rightarrow Mg_3BN_3(H)$. Further support for the double-bonded N=B=N species is found in maximum-entropy electron density maps calculated using the 34 observed structure factors with phases from the model (Hiraguchi *et al.*, 1991). The appreciably shallow valley observed between the N(2) and B atoms is ascribable to the bonding electrons of N=B=N.

The authors are grateful to N. Ishizawa who provided access to the JEOL diffractometer. Thanks are due to Daniel Louër for a copy of *DICVOL*91. Assistance with the draft preparation from N. Sudo is appreciated.

References

BOULTIF, A. & LOUËR, D. (1991). *J. Appl. Cryst.* **24**, 987–993.

CASCARANO, G., FAVIA, L. & GIACOVAZZO, C. (1992). *J. Appl. Cryst.* **25**, 310–317.

ELYUTIN, V. P., POLUSHIN, N. I., BURDINA, K. P., POLYAKOV, V. P., KALASHNIKOV, YA. A., SEMENENKO, K. N. & PAVLOV, YU. A. (1981). *Dokl. Akad. Nauk USSR*, **259**, 112–116; English translation (1981). *Dokl. Chem.* **259**, 290–294.

ENDO, T., FUKUNAGA, O. & IWATA, M. (1979). *J. Mater. Sci.* **14**, 1676–1680.

ESTERMANN, M. & GRAMLICH, V. (1992). *Accuracy in Powder Diffraction* II, NIST Special Publication 846, edited by E. PRINCE & J. K. STALICK, p. 26. Gaithersburg: National Institute of Standards and Technology.

GILMORE, C., HENDERSON, K. & BRICOGNE, G. (1991). *Acta Cryst.* A**47**, 830–841.

HIRAGUCHI, H., HASHIZUME, H., FUKUNAGA, O., TAKENAKA, A. & SAKATA, M. (1991). *J. Appl. Cryst.* **24**, 286–292.

HOHLFELD, C. (1989). *J. Mater. Sci. Lett.* **8**, 1082–1084.

JANSEN, J., PESCHAR, R. & SCHENK, H. (1992). *J. Appl. Cryst.* **25**, 237–243.

MCCUSKER, L. (1988). *J. Appl. Cryst.* **21**, 305–310.

MCCUSKER, L. (1992). *Accuracy in Powder Diffraction* II, NIST Special Publication 846, edited by E. PRINCE & J. K. STALICK, pp. 75–79. Gaithersburg: National Institute of Standards and Technology.

NAKANO, S., IKAWA, H. & FUKUNAGA, O. (1992). *J. Am. Ceram. Soc.* **75**, 240–243.

PYYKKÖ, P. & ZHAO, Y. (1990). *J. Phys. Chem.* **94**, 7753–7759.

SATO, T. (1986). *Res. Rep. Natl Inst. Res. Inorg. Mater.* No. 46, 53–56.

TAKEMURA, K., MINOMURA, S., SHIMOMURA, O. & FUJII, Y. (1980). *Phys. Rev. Lett.* **45**, 1881–1884.

TORAYA, H. (1986). *J. Appl. Cryst.* **19**, 440–447.

TORAYA, H. & MARUMO, F. (1980). *Rep. RLEMTIT. Tokyo Inst. Technol.* **5**, 55–64.

WENTROF, R. H. JR (1961). *J. Chem. Phys.* **34**, 809–812.

Acta Cryst. (1993). B**49**, 483–491

Phase Transition in $Sr_8[Al_{12}O_{24}](MoO_4)_2$ Aluminate Sodalite (SAM)

BY W. DEPMEIER,* R. MELZER† AND X. HU†

*Institut für Mineralogie und Kristallographie, TU Berlin, D-W-*1000 *Berlin* 12, *Germany*

(*Received* 3 *March* 1992; *accepted* 21 *December* 1992)

Abstract

The cubic–tetragonal phase transition at 571 K of the aluminate sodalite $Sr_8[Al_{12}O_{24}](MoO_4)_2$ (SAM) has been studied by following the position of the (pseudo-)cubic {400} reflections as a function of temperature. The high resolution of the synchrotron powder diffraction experiment allowed the temperature dependencies to be followed with good precision. The tetragonal **a** lattice parameter appears to be a linear extrapolation of the cubic one, with only a small upward shift at the transition, whereas the **c** parameter decreases strongly below 571 K. These observations can be explained by a model which assumes the superposition of a ferroelastic strain component, and a volume strain component. The volume strain can be rationalized as being the result of a 'shearing' of the sodalite framework. Causes and consequences of the 'shearing' in relation to the sodalite framework are discussed. The weakly first-order transition is nearly tricritical; power-law exponents seem to be influenced by defects. The thermal expansion of the cubic lattice parameter, as well as of the tetragonal **a** axis, is nearly linear. The linear thermal-expansion coefficient α is $8.6\,(4) \times 10^{-6}\,K^{-1}$. The tetragonal **c** axis also expands linearly between room temperature and about $T_c - 100$ K with practically the same coefficient, but behaves non-linearly nearer to the transition temperature.

Introduction

Aluminate sodalites of the general formula $M_8[Al_{12}O_{24}](XO_4)_2$, where X = S, Cr, Mo, W, ... and M represents Ca or Sr, have been studied in our group for some time (Depmeier, 1988). For all pure end members of the family, one or more structural phase transitions have been identified by various methods (Depmeier, 1988). It was found that most of the phase transitions are of ferroic character. For the title compound, $Sr_8[Al_{12}O_{24}](MoO_4)_2$ (SAM for short), in particular, a temperature-dependent neutron powder diffraction study revealed the

* Present address: Mineralogisches Institut, Universität Kiel, D-W-2300 Kiel 1, Germany.

† Present address: Hahn-Meitner-Institut, Glienicker Str. 100, D-W-1000 Berlin 39, Germany.

0108-7681/93/030483-09$06.00